

# Modeling and simulation of the nanosecond pulsed laser engraving process

*Evangelos Nikolidakis*<sup>1</sup>, *Aristomenis Antoniadis*<sup>1,\*</sup>

<sup>1</sup>School of Production Engineering & Management, Micromachining & Manufacturing Modeling Lab, University Campus Kounoupidiana, Technical University of Crete, 73100 Chania, Greece

**Abstract.** In this paper a 3D finite element simulation model of the nanosecond pulsed laser engraving process will be presented. With this model simulations of laser engraving process will be performed for some widely used materials using a wide range of process parameters in order to estimate the removed material layer thickness at each laser scan over the surface of the workpiece. Determining the removed material layer thickness is an important task because the machine must receive this value as input from the operator to calculate how many passes-layers need to be made in order to achieve the desired final depth of engraving. Since there is no simulation tool for this purpose at this time, the removed material layer thickness is determined through an experimental procedure. However, this procedure is time consuming as it has to be carried out each time separately depending on the process parameters, the material used, etc.

## 1 Introduction

Laser engraving is a machining process that achieves a high degree of precision compared to other traditional methods such as micro-machining with cutting tools. During laser engraving process, a laser machine generates laser beam pulses which impinge the target material surface. Each laser pulse ablates a very small amount of material. In order to produce the desired 3D geometry, the laser beam is scanned across the surface of the workpiece, sending the pulses at predefined positions. The quality of the result depends on the laser beam type, the workpiece material, the scanning strategy, the process parameters selection, etc. In order to correctly select the machining parameters and predict the machining result or final workpiece, the need to develop simulation tools was created.

Modeling and numerical simulation of laser engraving process is a complex task. Therefore, many researchers have dealt with modeling and numerical simulation of the laser ablation process of the materials. Wang et al. [1] proposed a two-dimensional (2D) modeling and simulation of the pulsed laser ablation process of aluminium caused by a single pulse using Abaqus Finite Element Analysis (FEA) software. R V Davydov and V I Antonov [2] presented a mathematical model for femtosecond laser ablation of metals. Roth et al. [3] presented a simulation model of femtosecond laser ablation in aluminium using double

---

\* Corresponding author: [antoniadis@dpem.tuc.gr](mailto:antoniadis@dpem.tuc.gr)

pulses. Tani et al. [4] developed a simulation package for micro-manufacturing processes using nanosecond pulsed lasers. L Dasallas and W Garcia [5] generated a numerical model of laser ablation process of copper caused by a femtosecond laser pulse at an oblique angle of incidence. T Hurtony [6] created a simulation tool for laser ablation caused by a single pulse shot in Matlab numerical computing environment. Aghaei et al. [7] presented a one-dimensional (1D) mathematical thermal model for a nanosecond pulsed laser ablation of copper in helium ambient gas.

In this work an experimentally confirmed 3D finite element simulation model of the nanosecond pulsed laser engraving process will be presented. Using this model the final 3d engraved geometry will be predicted taking into account the workpiece material properties, the laser machine process parameters, the interaction between the laser beam pulses and the irradiated target material, the ablation process mechanism, the material vapour-plasma formation and the laser beam shielding. Furthermore, the removed material layer thickness will be calculated using the predicted 3d final engraved geometry. The prediction of the removed material layer thickness is a major challenge because the laser machine must receive this value as input from the operator to calculate how many passes-layers  $n$  need to be made in order to achieve the desired final depth of engraving. Since there is no simulation tool for this purpose until now, the removed material layer thickness is determined through an experimental procedure. However, this procedure is time consuming as it has to be carried out each time separately depending on the process parameters, the material used, etc. and requires a remnant of the workpiece material for the experiments.

## 2 Modeling

### 2.1 Thermal model

For the thermal model of the laser beam a 2D surface Gaussian heat flux model was adopted [8]. The reason a surface heat flux model was chosen is that for nanosecond laser pulses on metals the absorption-penetration depth is very small as compared to the lateral heat diffusion dimensions of laser beam [9].

For the engraving of a 3D geometry laser beam pulses scan the surface of the workpiece moving on straight tracks and on multiple layers in a predetermined way (laser map). The laser map includes the coordinates of the focal point of the beam as well as the beam power  $P$  at each time point of the laser beam processing. As far as the laser power  $P$  as function of time, it was assumed that repeated pulses are generated with power equal to peak power [10,11] using a period step function. In order to generate the laser map the scanning strategy being used is cross hatching with hatching distance  $H_d$  to be equal with the track distance  $T_d$  and calculated by dividing the is the scanning speed  $V$  with the repetition rate  $F$  [12].

In order to calculate the energy absorbed by the target material coming from the incident laser beam, three cases are distinguished depending on the phase of the material as shown in Fig. 1.a. The first case shown on Fig. 1.a.1, the laser beam irradiates the target material and it's temperature is still below the melting temperature and the material is in solid phase. At this case, only a smart portion of the laser energy is absorbed by the surface of the material and the rest is reflected to the environment. The reflectivity of the laser beam on the metals is an optical property of the material and depends on the laser wavelength [13], the temperature and phase of the material (solid or liquid) [14] and is quite high for the most materials. Aluminium and brass reflects almost 95% of the radiation from Nd:YAG 1064nm laser beam at its solid phase. The second case shown on Fig. 1.a.2, the irradiated target material temperature has exceeded it's melting temperature but has not reached its evaporating temperature. That means that the material which absorbs the incident laser beam

is in liquid phase. The reflectivity of aluminium, copper and other reflective materials drops sharply once the material melts [15,16].

The third case shown on Fig. 1.a.3 the laser ablation has begun. The irradiated target material has reached it's ablation temperature which means that the target material is in liquid phase and simultaneously material vapour is generated [17] from the ablated material. As the generated material vapour above the surface interacts with the laser beam it absorbs a part of energy (laser beam shielding) [18,19] causing it's ionization and a high temperature and high electron density plasma is formed [20]. The radiation absorbed by plasma during shielding increases the thermal energy of the plasma and this results in plasma emitting irradiance itself, a part of which returns to the workpiece and is absorbed by the material.

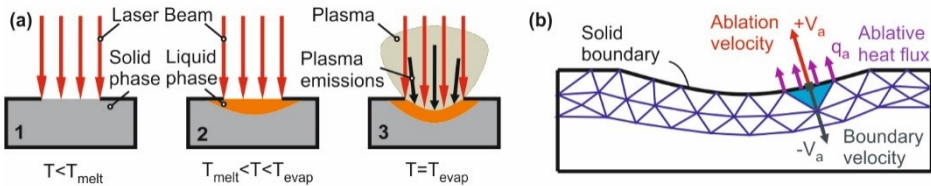


**Fig. 1. (a)** Ablation process thermal model **(b)** Laser ablation and material removal modeling

## 2.2 Material removal

Through the laser beam, the target material is being heated, leading to an increase in its temperature locally until it reaches the ablation temperature. When the surface material is at its ablation temperature there is mass loss from the surface and simultaneously a heat loss occurs due to the removal of the material vapor. The outward heat flux duo to material removal is governed by the mass flux of the ablated material and the heat of sublimation as follows:

$$q_a = M_a H_s, M_a = \rho v_a \tag{1}$$

where  $q_a$  is the ablative heat flux,  $M_a$  is the ablated material mass flux,  $H_s$  is the heat of sublimation,  $\rho$  is the material density and  $v_a$  is the material ablation velocity which has equal magnitude and opposite direction to the velocity of the solid boundary as shown in Fig. 1.b. Aiming at calculating the ablative heat flux at each iteration during finite elements analysis the heat-transfer version of Newton's law is used. The ablative heat flux is expressed as:

$$q_a = h_a(T_a - T) \tag{2}$$

where  $T_a$  is the ablation temperature and  $T$  is the temperature at each FEA iteration. A fictional temperature dependent heat transfer coefficient  $h_a$  is introduced that is zero for  $T < T_a$  and increases linearly with a very steep slope for  $T > T_a$ , in order to ensure that the temperature of the solid cannot exceed the ablation temperature. By combining the two above equations, at each iteration of the finite element analysis solving, the velocity at which the boundary surface of the grid must be moved is calculated. So, by calculating the mesh displacement of the moving front boundary at each iteration, the final geometry of the workpiece for each time step is obtained.

## 2.3 Initial geometry, material, initial-boundary conditions and meshing

For the simulations, a rectangular block was used as initial geometry whose dimensions were adjusted so that there is enough space to be engraved the rectangular pocket. The materials for which the model was built and tested as presented in this work are yellow bronze C26000 and aluminium 7075. The initial temperature  $T_0$  of the geometry was set to be equal to the ambient temperature  $T_0 = T_{amb}$ . As far as the boundary conditions, the top surface that

is heated by the laser beam was set to be a diffuse surface (only surface to ambient radiation). All the other surfaces were considered to have prescribed temperature  $T = T_{amb}$  (Dirichlet condition). For meshing the 3D geometry tetrahedral elements were used. In order to achieve mesh independent solutions, for the simulation tests a mesh with maximum element size of  $5\mu\text{m}$  with denser distribution in the direction of depth was chosen by performing a mesh independence study.

### 3 Simulation and experimental tests

Using the model presented above, a large number of simulations were performed to verify its proper operation and accuracy. As initial workpiece a rectangular block made by yellow brass C26000 or aluminium 7075 was used and the requested geometry was a  $150 \times 150 \mu\text{m}$  rectangular pocket made by four-layer laser beam scans-passes. Regarding the process parameters, cases were examined for average power  $P=8, 12, 16\text{W}$ , for repetition rate  $F=20, 30, 40\text{kHz}$  and scanning speed  $V=200, 300, 400, 500\text{ mm/s}$ . The simulation's output-result was the 3D engraved final workpiece geometry at all intermediate stages of processing, as would have occurred if the actual process carried out. From the exported 3D geometry it can be easily calculated the removed material layer thickness  $D_z$  by dividing the whole depth of the pocket  $D_{zn}$  by the number of the layers  $n$ . The removed material layer thickness  $D_z$  is the average thickness of the material removed on each laser beam scan-pass.

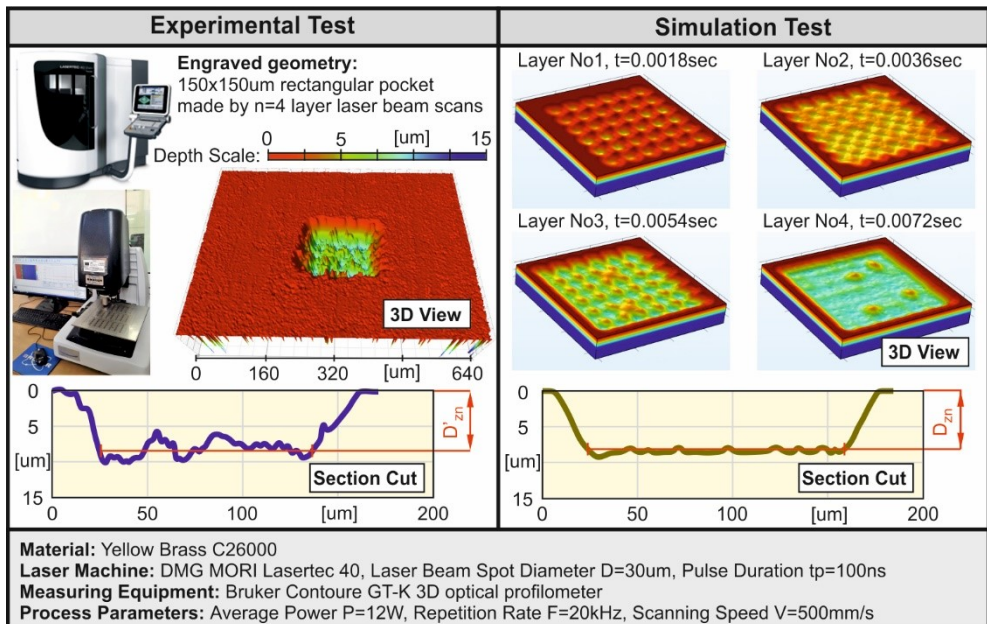


Fig. 2. Presentation of experimental test compared to simulation test

A set of experiments was performed for the purpose of comparing the experimental with the simulation results. The laser engraving experimental samples were conducted using the DMG MORI Lasertec 40 machine with spot diameter  $D=30\mu\text{m}$  and pulse duration  $t_{pulse}=100\text{ns}$  in 5mm thickness yellow brass C26000 and aluminium 7075 plates. The process was performed in exactly the same way as in the simulations. The sample geometry was a  $4 \times 4\text{mm}$  square pocket engraved by a constant number of 50 layers for brass and 30 layers for aluminium (number of layers selected to prevent engraving depth reach the whole plate thickness). The whole depth of each pocket measured using the Bruker Contour GT-K 3D

optical profilometer and the laser machine probing system was divided by the number of layers  $n$  to calculate the removed material layer thickness. In Fig. 2 is presented an example of a simulation test and the corresponding experimental test. The whole depth of the simulated pocket was predicted through the simulation to be  $D_{zn}=8.072\mu\text{m}$  and the corresponding one of the engraved pocket was measured by the optical profilometer to be  $D'_{zn}=8.210\mu\text{m}$ .

The removed material layer thickness from the experimental and the corresponding simulation tests are presented in Fig. 3 for brass and aluminium. By observing the diagrams in Fig.3 it becomes apparent that the numerical values are in agreement with the experimental ones. Not only are the numerical points close to the experimental ones, but the curves have the same tendency. In addition, from the diagrams some basic conclusions can be drawn about the effect of process parameters on removed material layer thickness: Power as a process parameter has a great bearing on the results of machining as it is observed that a slight increase in power  $P$  results in a significant increase in depth  $D_z$ . An equally important parameter can be considered speed as a small increase in scanning speed  $V$  results in a significant decrease in removed material layer thickness  $D_z$ . As far as the repetition rate  $F$  is concerned, the diagrams show that its effect on the removed material layer thickness  $D_z$  is not very significant as it does not cause any noticeable change in it, which may be due to the limited number of experiments.

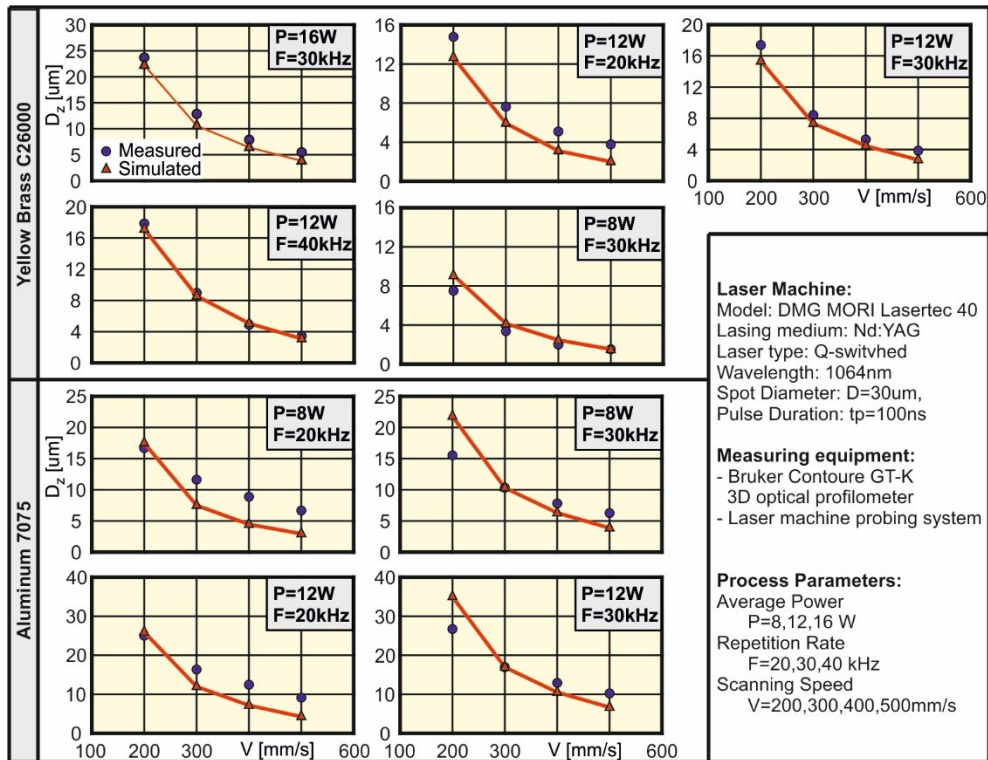


Fig. 3 Removed material layer thickness  $D_z$

## 4 Conclusions

In this paper, a 3D simulation model for laser engraving process in nanosecond fields using finite element method (FEM) was presented. At first, it was developed the laser map of the

laser engraving process which represents the timing and the positioning points of the pulses to be generated in order to be engraved the desired geometry. Then, the incident laser beam which provides the energy to cause the material ablation was modelled using a surface Gaussian distributed heat source. During the ablation process, the interaction between the laser beam and the material vapour-plasma was taken into account. The geometry shape change by ablated material removal was modeled by coupling heat conduction problem equations with the moving front boundary equations. A large number of simulations were performed for the case of engraving a rectangular pocket in yellow brass C26000 and aluminium 7075 for various values of process parameters: average power, repetition rate and scanning speed. The simulation's output-result was the 3D final workpiece geometry with the engraved pocket on it and the removed material layer thickness during the laser processing. Experimental tests were also performed using DMG MORI Lasertec 40 laser machine. The experimental results were compared with the numerical ones showing great agreement between them.

This research is co-financed by Greece and the European Union (European Social Fund- ESF) through the Operational Programme «Human Resources Development, Education and Lifelong Learning» in the context of the project “Strengthening Human Resources Research Potential via Doctorate Research – 2nd Cycle” (MIS-5000432), implemented by the State Scholarships Foundation (IKY).

## References

1. Y. Wang, N. Shen, G.K. Befekadu, C.L. Pasilio, *Int. J. Heat Mass Transf.* **113**, 1246 (2017).
2. R. V. Davydov, V.I. Antonov, *J. Phys. Conf. Ser.* **769**, 1 (2016)
3. J. Roth, A. Krauß, J. Lotze, H.R. Trebin, *Appl. Phys. A Mater. Sci. Process.* **117**, 2207 (2014).
4. G. Tani, A. Fortunato, L. Orazi, G. Cuccolini, *Int. J. Nanomanuf.* **3**, 279 (2009)
5. L.L. Dasallas, W.O. Garcia, *Mater. Res. Express.* **5**, 1 (2018)
6. T. Hurtony, 31st Int. Spring Semin. Electron. Technol. Reliab. Life-Time Predict. ISSE 2008. (2008)
7. M. Aghaei, S. Mehrabian, S.H. Tavassoli, *J. Appl. Phys.* **104**, 5 (2008).
8. A. Maleki, M. Kavosh Tehrani, H. Saghafifar, M.H. Moghtader Dindarlu, *Chinese Phys. B.* **25**, 3 (2016).
9. J.G. Lunney, R. Jordan, *Appl. Surf. Sci.* **127–129**, 941 (1998)
10. M.J. Kim, J. Zhang, *Appl. Math. Model.* **25**, 203-220 (2001).
11. K.A. Ghany, H.A. Rafea, M. Newishy, *Int. J. Adv. Manuf. Technol.* **28**, 1111 (2006).
12. D. Teixidor, I. Ferrer, J. Ciurana, T. Özel, *Robot. Comput. Integr. Manuf.* **29**, 209 (2013).
13. M.M. Quazi, M.A. Fazal, A.S.M.A. Haseeb, F. Yusof, H.H. Masjuki, A. Arslan, *Crit. Rev. Solid State Mater. Sci.* **41** (2016).
14. J. Xie, A. Kar, *Weld. J. (Miami, Fla.)* **78** (1999).
15. O. Benavides, O. Lebedeva, V. Golikov, *Opt. Express.* **19**, 21842 (2011).
16. O. Benavides, L. de la C. May, A.F. Gil, *Opt. Express.* **21**, 13068 (2013).
17. M. Aden, E. Beyer, G. Herziger, H. Kunze, *J. Phys. D. Appl. Phys.* **25**, 1 (1992).
18. N.M. Bulgakova, A. V. Bulgakov, *Appl. Phys. A Mater. Sci. Process.* **73**, 199 (2001).
19. R.K. Singh, O.W. Holland, J. Narayan, *J. Appl. Phys.* **68**, 233 (1990).
20. J.M. Vadiillo, J.M. Fernández Romero, C. Rodríguez, J.J. Surf. Interface Anal. **27** (1999).